Open Access

Journal of Energy and Power Technology

LIDSEN Publishing Inc.

Original Research

Fixed-Switching Frequency Finite-State Model Predictive Thrust and Primary Flux Linkage Control for LIM

Mahmoud F. Elmorshedy [1, 2, †], Abualkasim Bakeer [3, †, *], Dhafer Almakhles [1]

1. Renewable Energy Lab., College of Engineering, Prince Sultan University, Riyadh, Saudi Arabia; E-Mails: mahmoud.elmorshedy@f-eng.tanta.edu.eg; dalmakhles@psu.edu.sa
2. Electrical Power and Machines Engineering Department, Faculty of Engineering, Tanta University, Tanta, Egypt
3. Department of Electrical Engineering, Faculty of Engineering, Aswan University, Aswan 81542, Egypt; E-Mail: abualkasim.bakeer@aswu.edu.eg

† These authors contributed equally to this work.

* **Correspondence:** Abualkasim Bakeer; E-Mail: abualkasim.bakeer@aswu.edu.eg

Academic Editor: Mohammad Jafari

Special Issue: Optimal Energy Management and Control of Renewable Energy Systems

Journal of Energy and Power Technology
2023, volume 5, issue 2
doi:10.21926/jept.2302017

Received: February 14, 2023
Accepted: April 27, 2023
Published: May 09, 2023

Abstract

The special design of linear induction machines (LIMs) leads to adverse effects caused by the longitudinal and end effects. These effects make the thrust control of the LIMs most attractive because its value decreases sharply with the speed increase. Thus, finite-state model predictive control (FS-MPC) is developed to increase the performance of the LIMs. However, the variable switching frequency is the main drawback of this control. Consequently, the main objectives of this paper are to propose FS-MPC with a constant switching frequency, directly control the linear speed, and overcome the problems resulting from the longitudinal and end effects. Therefore, the proposed FS-MPC is based on the thrust and primary flux linkage (TF) control concept. In addition, the end effect is considered during the modeling of the proposed control method. The proposed FS-MPTFC method has been tested under different working cases using MATLAB/Simulink to check its validity. Parameters of a 3 kW arc induction machine have been used during the simulation results.

Keywords
Linear induction motor; finite-state model predictive control; thrust control; flux control; speed control

1. Introduction

In general, linear induction machines (LIMs) are created by cutting apart the rotor and stator of rotary induction machines (RIMs) and flattening them. The RIMs have been widely used in applications such as drive systems like lifts, electric vehicles, renewable energy, and so on [1-6]. LIMs have many advantages and hence can be used in different applications. One of the most widespread applications is the employment of linear metro due to their substantial benefits of direct linear motion without any transformation gears, which can benefit from powerful acceleration or deceleration, outstanding hill-climbing ability, low noise, and so on [7-9]. The HSST in the Tobu-Kyuryo-Line, the Guangzhou Subway Line 4, the airport rapid transport line in China, the Kennedy Airline in America, the Vancouver light train in Canada, and others are just a few of the more than 30 commercial lines that have been built to date [10, 11]. However, the mutual inductance of LIM fluctuates with operation speed with significant nonlinear features, which is why it is thought that the primary problem with these machines is their end effects, which would negatively affect the drive performance of the entire system [12].

Up until now, the LIM and drive have primarily used field-oriented control (FOC) and direct thrust control (DTC) [13, 14]. The FOC generally has issues with changing parameters, transformation matrices, and delayed response, whereas the DTC has issues with high thrust ripple and variable switching frequency. To solve the issues with classical control, model predictive control (MPC) methodologies are proposed [15-17]. MPC is typically divided into two categories: continuous-state MPC (CS-MPC) and finite-state MPC (FS-MPC) [18]. In this work, the FS-MPC is used due to its straightforward implementation, quick dynamic reaction, and other factors after rigorous comparison [19-22]. In a nutshell, there are two forms of FS-MPC: FS-MPCC, which is based on predictive current control, and FS-MPTFC, which is based on predictive thrust and flux control [8, 23]. The long computation times caused by the Clark transformation are often the most significant FS-MPCC issues.

Therefore, the FS-MPTC has been developed and discussed widely in recent research work such as [24-31]. In [24] and [25], the speed estimation algorithm for the LIMs is proposed based on a model reference adaptive system (MRAS), while the FS-MPDTC is used as a controller. The FS-MPDTC with the speed estimation is used to improve the LIM drive system performance, where low cost, low thrust and flux ripple, and fast response can be achieved. In [25], fuzzy logic control (FLC) is adopted instead of the proportional integral control for both the outer speed control loop and the adaptation mechanism of the MRAS with a minimum number of membership functions to decrease the computation time.

In [26] and [27], the FS-MPC is improved for the LIMs to remove the weighting factor from the cost function and reduce the calculation burden. These proposed methods are called finite-state model predictive voltage control (FS-MPVC) and finite-state model predictive flux control (FS-MPFC). In [28], a comparison between the FS-MPTC and the FS-MPFC is presented to illustrate the capability of each control method. In [28] and [29], the sliding mode control is used in the outer control loop of the FS-MPTC for the LIMs and compared with the PI control loop. The target of combining the SMC with the FS-MPTC is higher tracking accuracy and faster error convergence. In [23], the FS-MPTC is improved to increase the efficiency of the LIMs by achieving the maximum thrust per ampere, where the optimum flux linkage is calculated according to the electromagnetic thrust and set as a reference in the cost function. In [30], the FS-MPTC is combined with the DTC concept to reduce the number of predicting voltage vectors and hence reduce the computation time.

Although extensive research works have been done to achieve and increase the performance of the LIMs drive system based on the FS-MPTC concept, all of these FS-MPTC are based on the variable switching frequency concept, which is not preferred for the three-phase voltage inverter as the inverter can be damaged if the switching frequency is increased above the allowable rating values.

As a result, this research suggests using a fixed-switching frequency in a finite state model predictive thrust and flux control to eliminate the problem of the variable switching frequency. The following are the main key points of the paper:

- Design a fixed-switching frequency finite state model predictive thrust and flux control for VSI-driven LIM.
- Define optimally the dwell times associated with the vectors of the selected sector.
- Provide high power quality for the VSI-driven LIM by fixing the switching frequency.
- Validate the proposed fixed-switching FS-MPTFC using MATLAB/Simulink software.

The structure of this essay is as follows: The mathematical model of the LIM is described in Section II. The conventional FS-MPTFC approach is presented in Section III. Section IV details the proposed approach of the fixed-switching frequency for FS-MPTFC. In Section V, simulation results are discussed to demonstrate that the proposed method can fix the switching frequency and improve poor performance brought on by variable switching frequency. Finally, section VI reports the conclusions of the paper.

2. LIM Mathematical Model

Researchers were concerned about the LIM's dynamic model due to the end-effect activities that cause the air-gap flux linkage to wander [10, 31]. Based on Duncan's equivalent circuit, the LIM's dynamic model is presented [31]. In [8], the entire dynamic model, including the end-effect, is displayed in $\alpha\beta$-axis coordinates. The following relations describe the modeling of the LIM in the stationary reference frame.

$$\left.\begin{aligned} u_{\alpha 1} &= R_{\alpha 1} i_{\alpha 1} + \frac{\mathrm{d}\lambda_{\alpha 1}}{dt} \\ u_{\beta 1} &= R_{\beta 1} i_{\beta 1} + \frac{\mathrm{d}\lambda_{\beta 1}}{dt} \end{aligned}\right\rangle \tag{1}$$

$$\left.\begin{aligned} 0 &= R_{\alpha 2} i_{\alpha 2} + \frac{d\lambda_{\alpha 2}}{dt} + (\omega_1 - \omega_2)\lambda_{\beta 2} \\ 0 &= R_{\beta 2} i_{\beta 2} + \frac{d\lambda_{\beta 2}}{dt} + (\omega_1 - \omega_2)\lambda_{\alpha 2} \end{aligned}\right\rangle \quad (2)$$

Where u_α, u_β are the $\alpha\beta$-axis voltages, i_α, i_β the $\alpha\beta$-axis currents, and λ_α, λ_β the $\alpha\beta$-axis flux-linkages. R is the resistance and L stands for self-inductance. Meanwhile ω_1 and ω_2 are the primary and the secondary linear speed, respectively. In the meantime, subscripts 1 and 2 refer to the primary and the secondary.

The $\alpha\beta$-axes of the primary and secondary flux-linkages are calculated from

$$\left.\begin{aligned} \lambda_{\alpha 1} &= L_1 i_{\alpha 1} + L_{meq} i_{\alpha 2} \\ \lambda_{\beta 1} &= L_1 i_{\beta 1} + L_{meq} i_{\beta 2} \end{aligned}\right\rangle \quad (3)$$

$$\left.\begin{aligned} \lambda_{\alpha 2} &= L_2 i_{\alpha 2} + L_{meq} i_{\alpha 1} \\ \lambda_{\beta 2} &= L_2 i_{\beta 2} + L_{meq} i_{\beta 1} \end{aligned}\right\rangle \quad (4)$$

In addition, L_{meq} is calculated using the mutual inductance after end-effect modification and is computed by

$$L_{meq} = \big(1 - f(Q)\big) L_m \quad (5)$$

where $f(Q)$ is a coefficient introduced by the dynamic end effect, and L_m is the mutual inductance at static. $f(Q)$ is the dynamic end-effect and it is calculated from

$$f(Q) = \frac{[1 - \exp(-Q)]}{Q} \text{ where } Q = \frac{D_s R_2}{(v_2[L_{l2} + L_m])} \quad (6)$$

The motion relation for the LIM is given by

$$F_e = F_l + M\frac{dv_2}{dt} + Bv_2 \quad (7)$$

Meanwhile, the electromagnetic thrust can be calculated from

$$F_e = \frac{3}{2}\frac{\pi}{\tau}\left(\vec{\lambda}_1^* \otimes \vec{i}_1\right) \quad (8)$$

3. Conventional Finite-State Model Predictive Thrust and Flux Control (FS-MPTFC)

FS-MPTFC is offered for the LIM to obtain a quicker response, reduced thrust ripples, and the lowest primary flux-linkage ripples. The FS-MPTFC operates on the same principles as the traditional DTC, except for using an already established switching table. However, the switching vector that provides a minimal value for the cost function is chosen by the FS-MPTFC. This control method can be broken down into three critical steps to maximize efficiency. The most important stage in selecting the best vector is parameter estimate, followed by the prediction step, and cost function optimization step. These key points are outlined below.

- The estimation step for both primary and secondary flux linkages is determined through the following relations:

$$\vec{\lambda}_1(k) = \vec{\lambda}_1(k-1) + Ts\big(\vec{v}_1(k) - R_1\vec{i}_1(k)\big) \tag{9}$$

$$\vec{\lambda}_2(k) = \frac{L_2}{L_{meq}}\vec{\lambda}_1(k) + \left(L_{meq} - \frac{L_2L_1}{L_{meq}}\right)\vec{i}_1(k) \tag{10}$$

- With the use of the first-order Euler technique, predictions for the primary flux-linkage, λ_1(k + 1), primary current, i_1(k + 1), and electromagnetic thrust, F_e(k + 1) are determined by

$$\lambda_{\alpha1,i}(k+1) = \lambda_{\alpha1}(k) + T_s\left(u_{\alpha1,i}(k) - R_1 i_{\alpha1}(k)\right) \tag{11}$$

$$\lambda_{\beta1,i}(k+1) = \lambda_{\beta1}(k) + T_s\left(u_{\beta1,i}(k) - R_1 i_{\beta1}(k)\right) \tag{12}$$

$$\begin{aligned} i_{\alpha1,k}(k+1) = [i_{\alpha1}(k)] \times \left[-\left(\frac{T_s}{Z}\right)\left(R_1 + \frac{R_2}{\tau_l^2}\right) + 1\right] \\ + \left(\frac{T_s}{Z}\right) \times \left(u_{\alpha1,k}(k) + \left(\frac{1}{\tau_r\tau_l} - \frac{\omega_2}{\tau_l}\right)\lambda_{\beta2}(k)\right) \end{aligned} \tag{13}$$

$$\begin{aligned} i_{\beta1,k}(k+1) = \left[-\left(\frac{T_s}{Z}\right)\left(R_1 + \frac{R_2}{\tau_l^2}\right) + 1\right] \times [i_{\beta1}(k)] \\ + \left(\frac{T_s}{Z}\right) \times \left(u_{\beta1,k}(k) + \left(\frac{1}{\tau_r\tau_l} - \frac{\omega_2}{\tau_l}\right)\lambda_{\alpha2}(k)\right) \end{aligned} \tag{14}$$

$$F_e(k+1) = \frac{3}{2}\frac{\pi}{\tau}\begin{pmatrix} \lambda_{\alpha1}(k+1) * i_{\beta1}(k+1) \\ +\lambda_{\beta1}(k+1) * i_{\alpha1}(k+1) \end{pmatrix} \tag{15}$$

whereas $\tau_r = \frac{L_2}{R_2}, Y = \frac{(T_S)}{[L_2+R_2T_S]}$, $Z = (L_1 - \frac{L_{meq}^2}{L_2})$, $\tau_l = \frac{L_2}{L_{meq}}$, $u_{\alpha,\ k}(k)$ and $u_{\beta,\ k}(k)$ are the *αβ*-axis voltage vectors. $i_{\alpha1}(k)$ and $i_{\beta1}(k)$ are the *αβ*-axis measured currents.

The proposed cost function, g_T, is designed as follows:

$$g_T = \left|F_e^* - F_{e,i}(k+1)\right| + K_1\left|\lambda_1^* - \lambda_{1,i}(k+1)\right| \tag{16}$$

where K_1 stands for the weighting factors. A single PI controller controls the linear speed, and the output of this PI is subsequently employed as a reference thrust in the cost function. The complete block diagram of the conventional FS-MPTFC is illustrated in Figure 1.

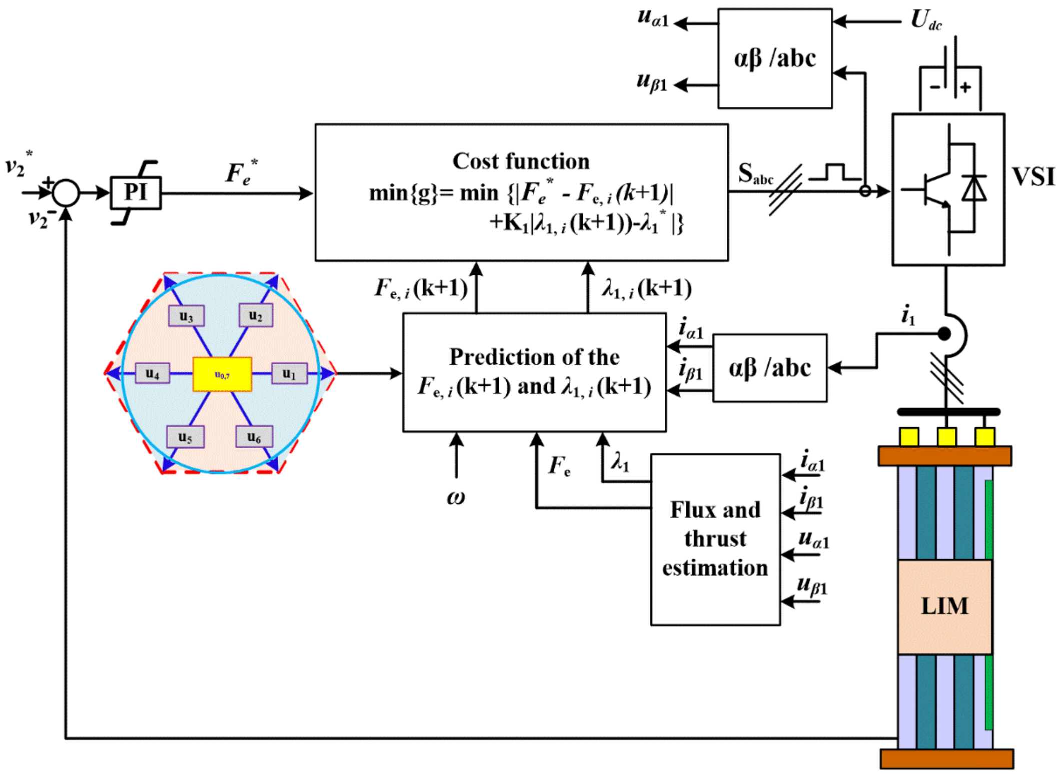

Figure 1 FS-MDTFC for the LIM drive system.

4. Proposed Fixed-Switching Frequency FS-MPTFC for LIM Drive System

As a result of space vector modulation, it is possible to precisely position each vector within the vector space information in the ($\alpha\beta$) plane, as shown in Figure 2. The ($\alpha\beta$) plane can be divided into six sectors, each corresponding to a certain direction. According to the proposed technique, the two active vectors that comprise each sector are calculated from the predicted values of the two active vectors (S_n where $n \in [1, 6]$) at every sampling time (T_s) and evaluates the total cost function.

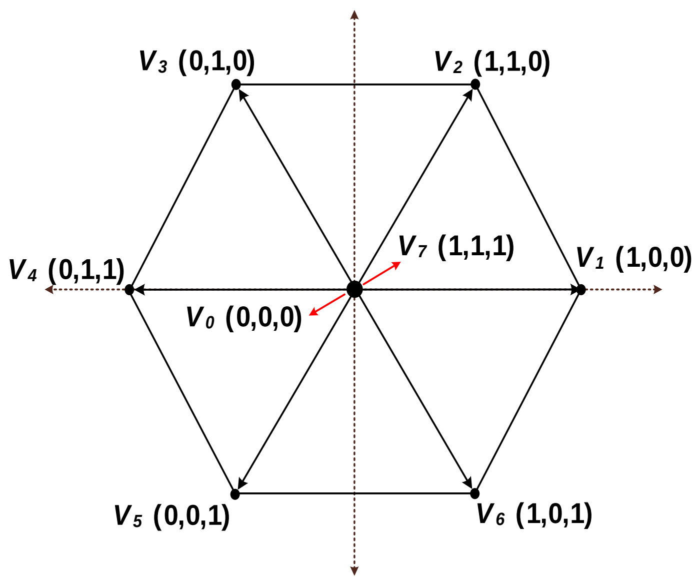

Figure 2 Space vectors of the output voltage at the 2L-VSI terminals.

The cost function measures the difference between the actual and predicted vector output. Next, the fixed-switching frequency FS-MPTFC uses this information to adjust the active vectors so that the predicted vector output matches the actual vector output. In the last step, the cost function for each sector is evaluated, and predictions are made, where duty cycles are calculated for active vectors and zero vectors using the following equation:

$$d_x = \frac{\delta}{J_x} \tag{17}$$

where δ denotes the proportionality constant, the subscript x refers to the adjacent vectors, in the current case (x = 1; 2) for the active vectors in the sector, while x = 0 corresponds to the zero vector.

The sum of the duty-cycle for the two active vectors and the zero vector is always equal to one; see Eq. (16) in which d_1 is the duty-cycle for the first active vector in the sector, d_2 is the duty-cycle of the second active vector in the sector, and d_0 is the duty-cycle of the zero vector. The value of the duty cycle for each voltage vector can be found by solving Eq. (15) and Eq. (16), yielding Eq. (17).

$$d_1 + d_2 + d_0 = 1 \tag{18}$$

$$\begin{cases} d_1 = \dfrac{\sigma J_2 J_0}{J_1 J_2 + \sigma J_1 J_0 + \sigma J_2 J_0} \\ d_2 = \dfrac{\sigma J_1 J_0}{J_1 J_2 + \sigma J_1 J_0 + \sigma J_2 J_0} \\ d_0 = \dfrac{J_1 J_2}{J_1 J_2 + \sigma J_1 J_0 + \sigma J_2 J_0} \end{cases} \tag{19}$$

A tuning parameter σ is associated with the cost function during the zero-voltage vector (i.e., J_0) [32]. Adjusting σ affects the zero-vector time and therefore affects the performance of the 2L-VSI on the LIM. In the current work, the value of the σ parameter is set employing trial and error until achieving the desired performance. At every time step t, the following cost function is evaluated to determine the optimal sector selection as

$$g(k+1) = d_1 J_1 + d_2 J_2 \tag{20}$$

where J_1 and J_2 are the cost functions associated with the tested sector's first and second voltage vectors, respectively.

The two vectors that minimize the cost function are chosen and applied in the next sampling interval. To determine how long each vector will be applied for in one sampling period, we need to find the corresponding time for each vector, which denotes the dwell time. This can be obtained by using the obtained duty cycle of each voltage vector in Eq. (17) and the value of the sampling time as:

$$\begin{cases} T_1 = d_1 T_s \\ T_2 = d_2 T_s \\ T_0 = d_0 T_s \end{cases} \tag{21}$$

After defining the optimal sector S_n and dwell time for each vector, the next step is distributing these vectors within one sampling interval. This is important so that the vector distribution is consistent over time. For example, when the optimal sector is odd (n = 1, 2, or 5), the switching sequence in Figure 3(a) should be followed. At the even optimal sector (that is n = 2, 4, or 6), the switching sequence in Figure 3(b) should be followed.

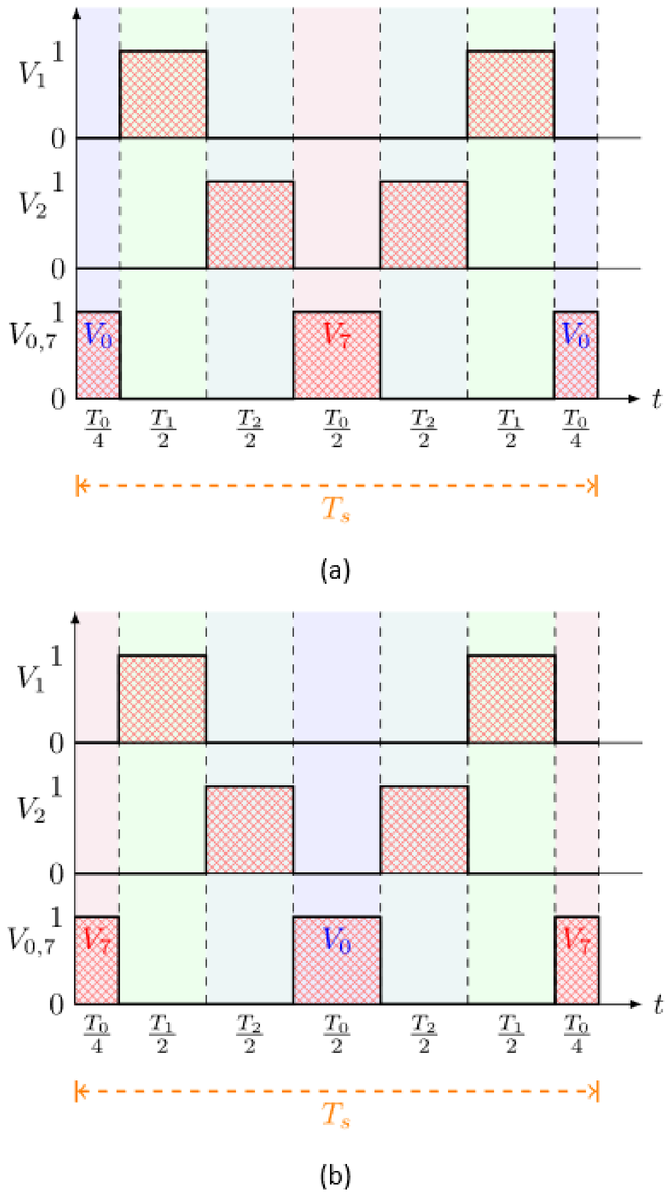

Figure 3 Switching pattern of the 2L-VSI vectors in the case of the optimal sector is a) odd and (b) even.

The complete flowchart of the proposed fixed-switching frequency FS-MPTFC for 2L-VSI loading with LIM is depicted in Figure 4. The proposed fixed-switching frequency FS-MPTFC begins by measuring the necessary measurements for predicting the control objectives. These measurements are filtered from the noise to improve accuracy. Next, the fixed-switching frequency FS-MPTFC stage generates an optimal switching sector and dwells time pattern, which is then fed to the SVPWM stage to generate the required switching pattern. As a result of the computational burdens of real-time implementation, applying the chosen switching state after the next sample instant is a simple solution to the delay [33, 34].

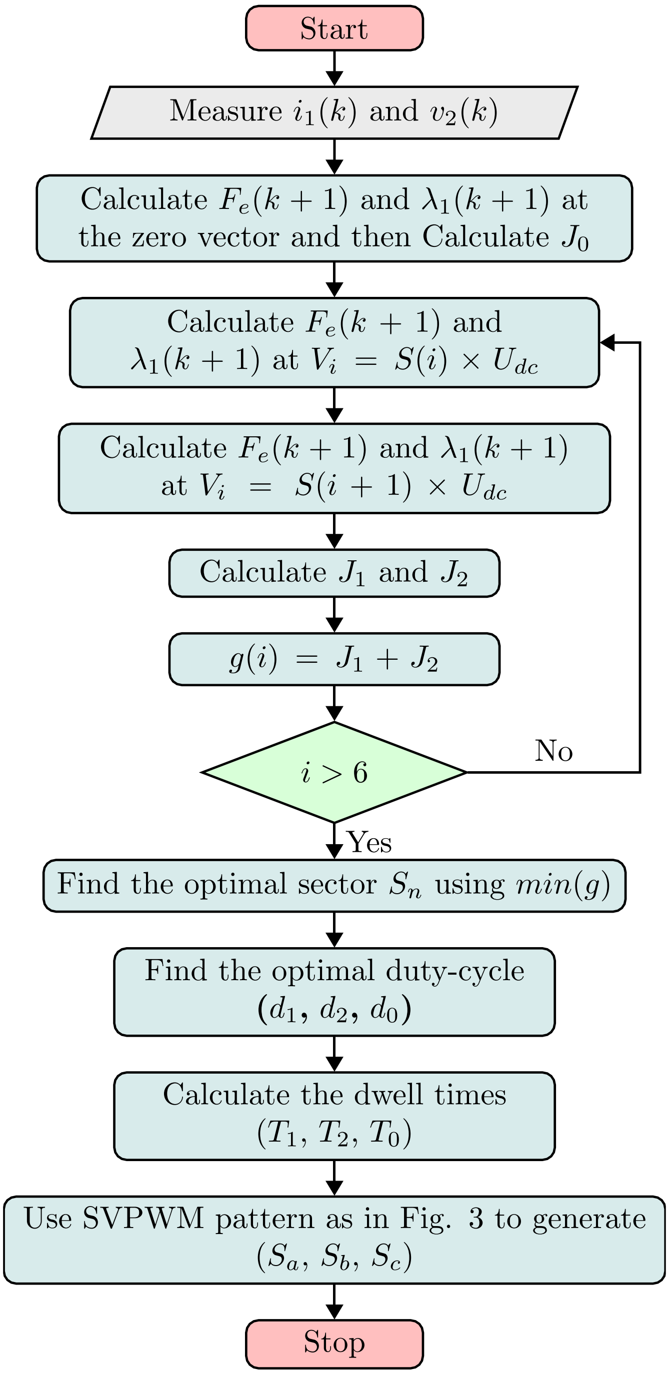

Figure 4 Flowchart of the proposed fixed-switching frequency FS-MDTFC for LIM driven by 2L-VSI.

5. Simulation Results

Dynamic analyses are used to prove that the proposed FS-MPTFC with fixed-switching frequency is viable. The essential arc induction machine (AIM) prototype characteristics are used to analyze the simulation results produced by the MATLAB/Simulink model. The data and parameters related to this AIM are listed in Table 1. This control strategy is tested under different reference speeds and sample load intervals to guarantee validity.

Table 1 LIM Parameters.

Quantity	Symbol	Value	Unit
Primary resistance	R_1	1	Ω
Secondary resistance	R_2	2.4	Ω
Primary leakage inductance	L_{l1}	0.0114	H
Secondary leakage inductance	L_{l2}	0.0043	H
Pole pitch	τ	0.1485	m
Nominal power	P_N	3	kW
Nominal thrust	F_N	280	N
Nominal current	I_N	22	A
Nominal voltage	U_N	180	V
Nominal speed	v_N	11	m/s

5.1 Speed Change Condition

The LIM drive system is tested using the suggested fixed-switching frequency FS-MPTFC with variable speed. Speed increases from 6 m/s to 8 m/s while the load remains constant at 50 N. As seen in Figure 5, the electromagnetic thrust created ensures that the appropriate thrust load is followed. At the same time, the actual speed tracks the reference value. Figure 6 depicts the dynamic response of the electromagnetic and load thrust. As seen from the -axis in Figure 7, the principal flux linkage is fixed at the reference value in the interim. Figure 8 displays the three-phase primary current's dynamic response. In addition, Figure 9 shows the three-phase voltage corresponding to the ideal switching vector with fixed-switching frequency. Finally, Figure 10 depicts the secondary flux linkage corresponding to the speed change.

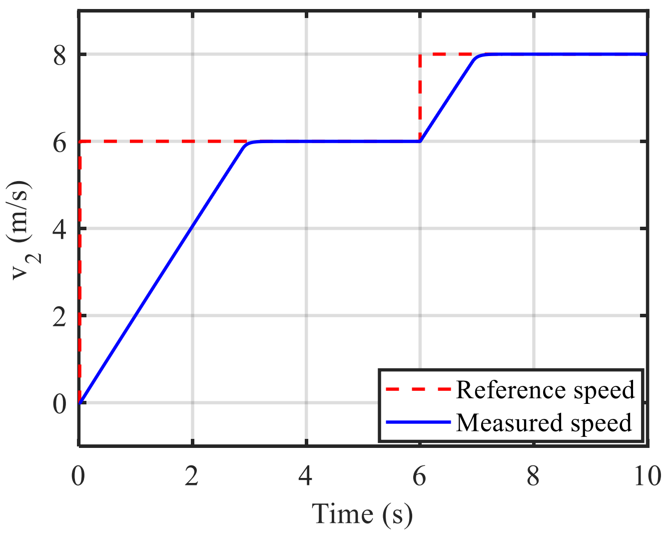

Figure 5 Dynamic response of reference and measured speed of the LIM.

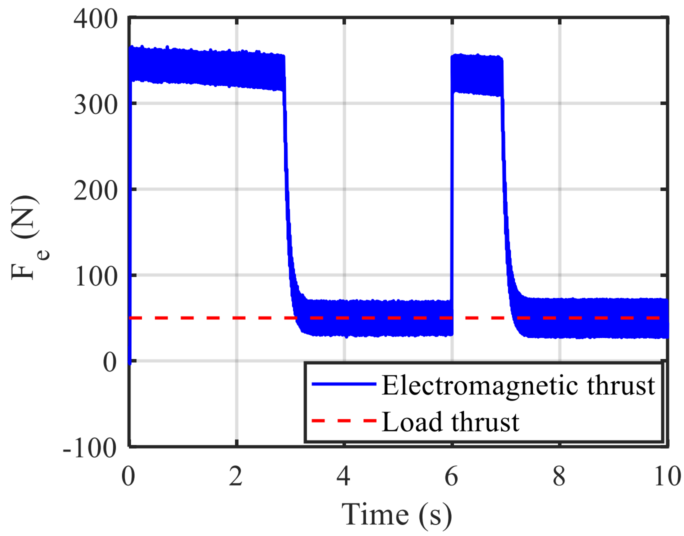

Figure 6 Dynamic response of the electromagnetic thrust during speed change of the LIM.

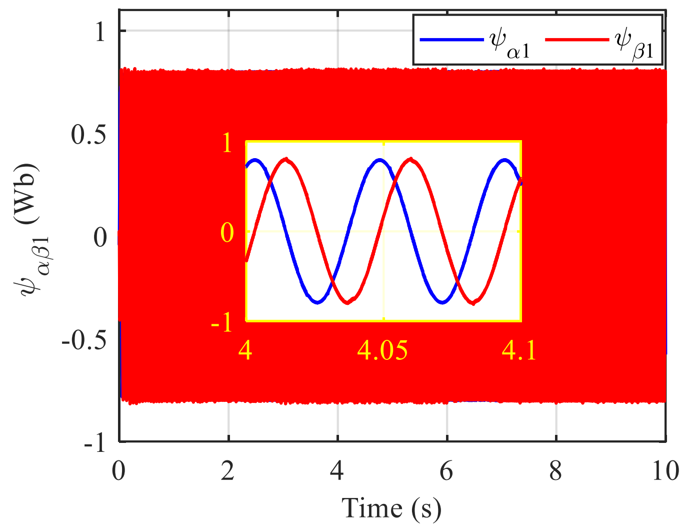

Figure 7 Dynamic response of the primary flux linkage during speed change of the LIM.

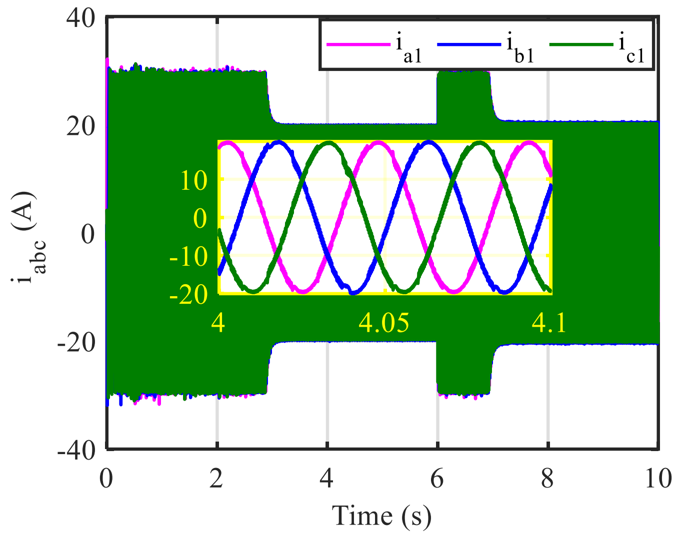

Figure 8 Dynamic response of the primary current during speed change of the LIM.

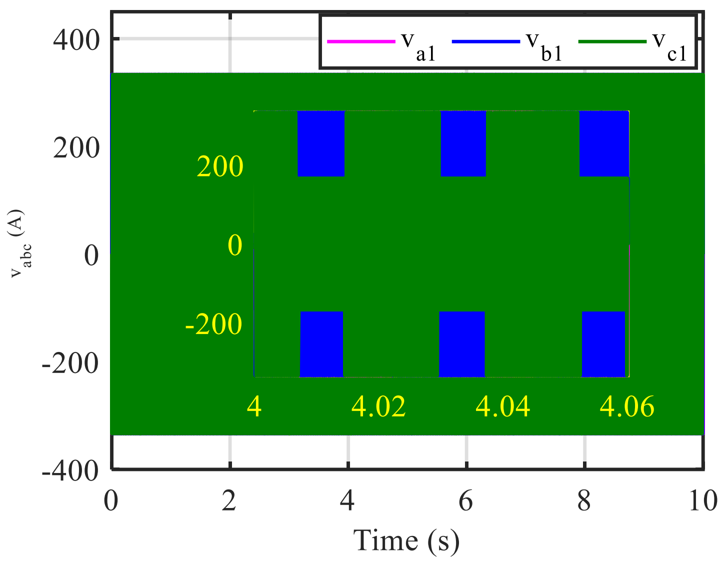

Figure 9 Output voltage corresponding to the optimum switching vectors during speed change of the LIM.

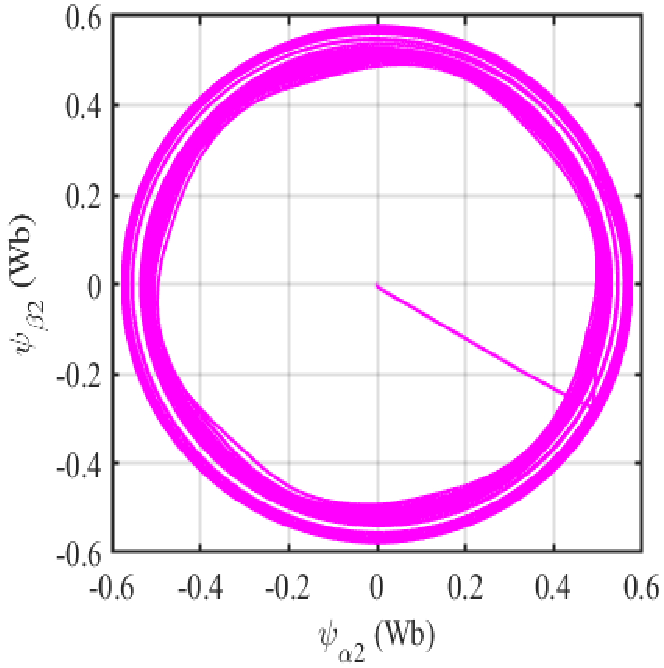

Figure 10 Dynamic response of the secondary flux linkage during speed change of the LIM.

5.2 Dynamic Performance of the Drive System under Load Change

In this scenario, the thrust load rise from 60 N up to 150 N while the reference speed remians constant at 7 m/s. Figure 11 and Figure 12 demonstrate the electromagnetic thrust and the speed response. The electromagnetic thrust is seen to match the necessary thrust load. The actual speed also follows the reference value. In addition, Figure 13 and Figure 14 display the three-phase current and voltages that correlate to the load variation. Finally, Figure 15 and Figure 16 show the primary and secondary flow linkages, respectively.

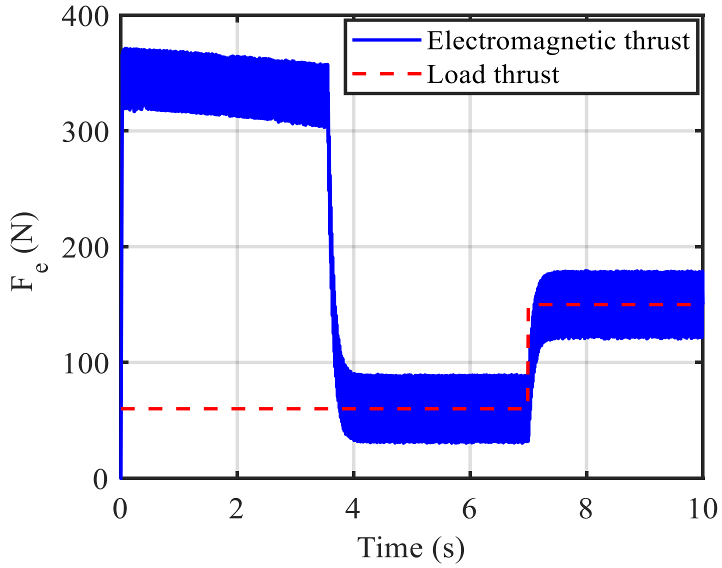

Figure 11 Dynamic response of the electromagnetic thrust during load thrust change of the LIM.

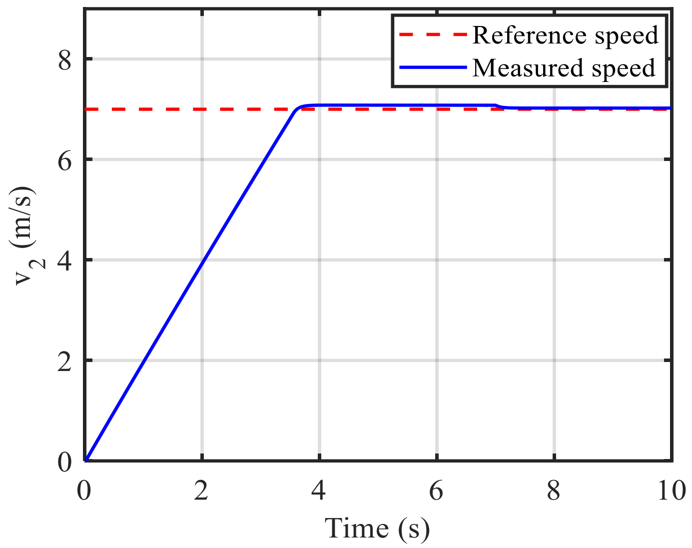

Figure 12 Dynamic response of the actual speed during the LIM load thrust change.

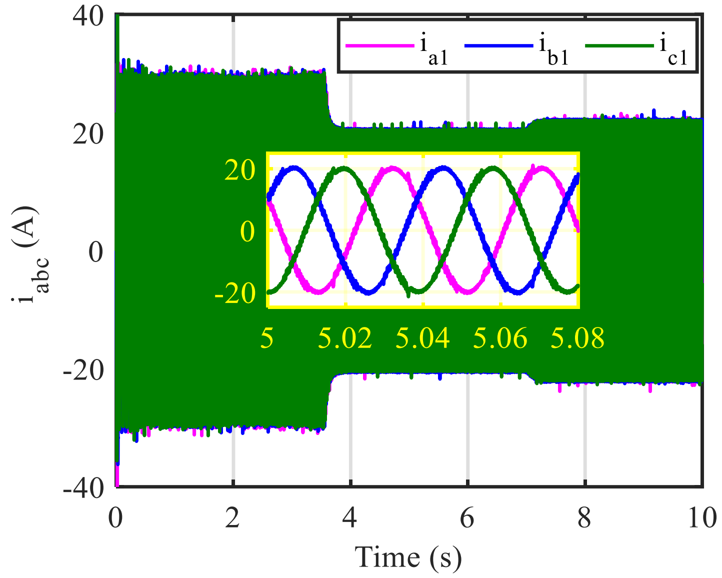

Figure 13 Dynamic response of the primary during load thrust change of the LIM.

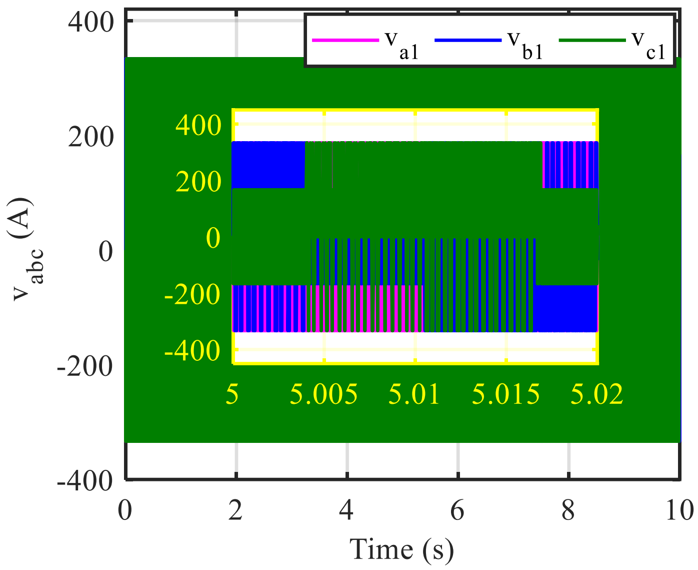

Figure 14 Output voltage corresponding to the optimum switching vectors during load thrust change of the LIM.

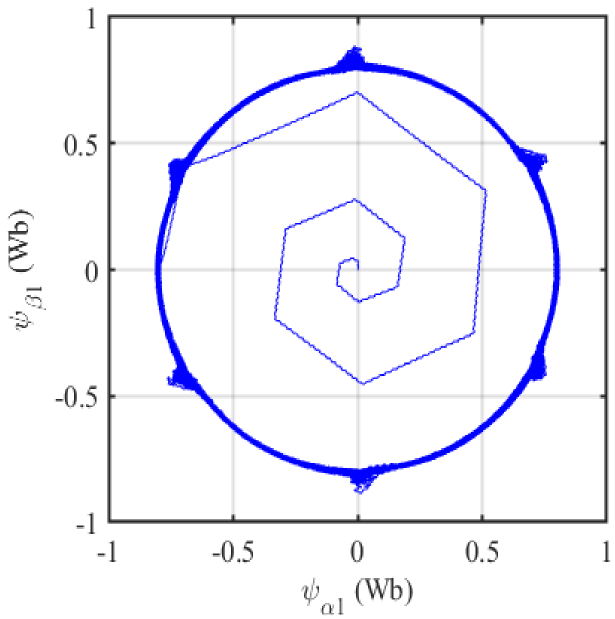

Figure 15 Dynamic response of the primary flux linkage during load thrust change of the LIM.

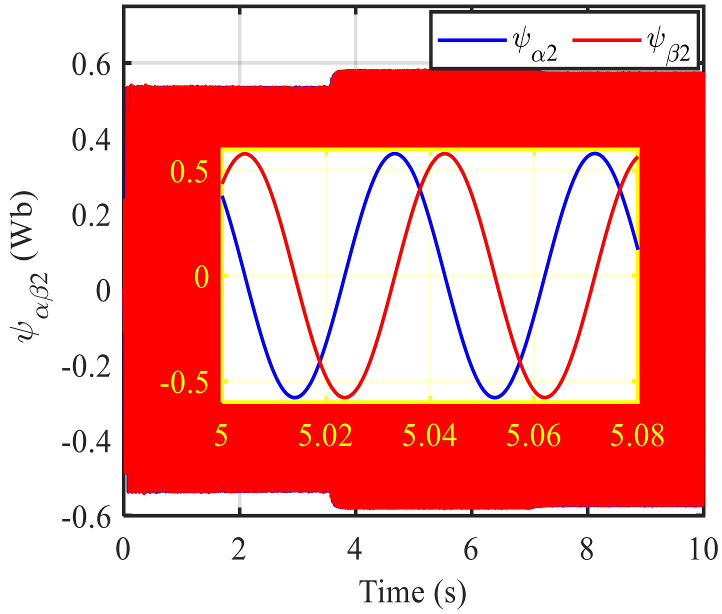

Figure 16 Dynamic response of the secondary flux linkage during load thrust change of the LIM.

5.3 Comparison between the Proposed Fixed-Switching FS-MPTFC and Conventional FS-MPTFC

The switching frequency characteristics in Figure 17a show that the VSI operates on a fixed frequency of 10 kHz with the proposed FS-MPTFC. Therefore, the harmonics spectrum appears when at multiplications of the switching frequency. On the other hand, the conventional FS-MPTFC has a wider harmonics spectrum, as shown in Figure 17b.

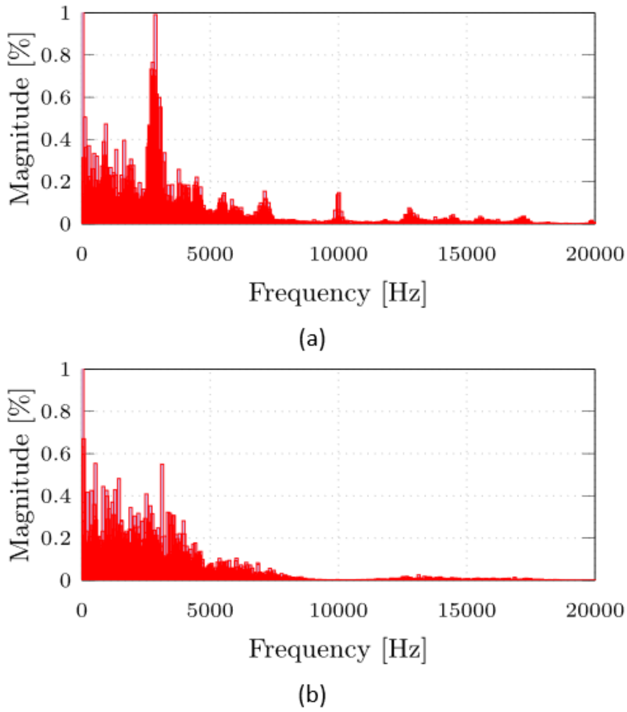

Figure 17 THD evaluation of the primary current: a) proposed fixed-switching FS-MPTFC, and b) conventional FS-MPTFC.

6. Conclusions

This research article proposes an improved finite-state model predictive thrust and primary flux linkage control (FS-MPTFC) for the linear induction machine used in the linear metro. The proposed FS-MPTFC solved the problem of the variable switching frequency existing in the conventional FS-MPTC control. The proposed FS-MPTFC is based on the fixed-switching frequency to protect the inverter from damage when a high switching frequency is generated and reduce the thrust and primary flux linkage ripples, increasing the linear metro drive system performance. In addition, the linear speed of the LIM is directly controlled by adding an external PI controller to the FS-MPTFC, where the output of this PI controller modifies the reference thrust to fast-track the changeable speed. Utilizing MATLAB/Simulink, the proposed control mechanism's validity has been examined, and the outcomes demonstrated the potential of the suggested control strategy to deliver the required performance.

Author Contributions

The authors contributed equally to this work.

Competing Interests

The authors have declared that no competing interests exist.

References

1. Rodriguez J, Garcia C, Mora A, Davari SA, Rodas J, Valencia DF, et al. Latest advances of model predictive control in electrical drives–Part II: Applications and benchmarking with classical control methods. IEEE Trans Power Electron. 2021; 37: 5047-5061.
2. Elmorshedy MF, Xu W, El-Sousy FF, Islam MR, Ahmed AA. Recent achievements in model predictive control techniques for industrial motor: A comprehensive state-of-the-art. IEEE Access. 2021; 9: 58170-58191.
3. Krishna VM, Sandeep V, Murthy SS, Yadlapati K. Experimental investigations on performance comparison of self excited induction generator and permanent magnet synchronous generator for small scale renewable applications. Renew Energy. 2022; 195: 431-441.
4. Duvvuri SS, Sandeep V, Yadlapati K, Krishna VM. Research on induction generators for isolated rural applications: State of art and experimental demonstration. Measurement. 2022; 24: 100541.
5. Rajak MK, Samanta J, Pudur R. A hardware-based novel approach for parallel operation of two differently rated SEIGs. Results Eng. 2023; 17: 100825.
6. Kumar RH, Iqbal A, Lenin NC. Review of recent advancements of direct torque control in induction motor drives-a decade of progress. IET Power Electron. 2018; 11: 1-15.
7. Hu D, Xu W, Dian R, Liu Y, Zhu J. Loss minimization control of linear induction motor drive for linear metros. IEEE Trans Ind Electron. 2018; 65: 6870-6880.
8. Xu W, Elmorshedy MF, Liu Y, Islam MR, Allam SM. Finite-set model predictive control based thrust maximization of linear induction motors used in linear metros. IEEE Trans Veh Technol. 2019; 68: 5443-5458.

9. Xu W, Zhu J, Guo Y, Tan L, Wang S. Analysis on performance of linear induction motor basing on winding function method. Proceedings of 2009 4th IEEE Conference on Industrial Electronics and Applications; 2009 May 25-27; Xi'an, China. Piscataway, New Jersey, United States: IEEE.
10. Xu W, Zhu JG, Zhang Y, Li Z, Li Y, Wang Y, et al. Equivalent circuits for single-sided linear induction motors. IEEE Trans Ind Appl. 2010; 46: 2410-2423.
11. Boldea I, Tutelea LN, Xu W, Pucci M. Linear electric machines, drives and MAGLEVs: An overview. IEEE Trans Ind Electron. 2017; 65: 7504-7515.
12. Alonge F, Cirrincione M, Pucci M, Sferlazza A. Input-output feedback linearization control with on-line MRAS-based inductor resistance estimation of linear induction motors including the dynamic end effects. IEEE Trans Ind Appl. 2016; 52: 254-266.
13. Wang K, Li Y, Ge Q, Shi L. An improved indirect field-oriented control scheme for linear induction motor traction drives. IEEE Trans Ind Electron. 2018; 65: 9928-9937.
14. Elmorshedy MF, Xu W, Liu Y. Speed control of linear induction motor with thrust and stator flux ripple reduction. Proceedings of 2018 21st International Conference on Electrical Machines and Systems (ICEMS); 2018 October 07-10; Jeju, Korea (South). Piscataway, New Jersey, United States: IEEE.
15. Mir TN, Singh B, Bhat AH. FS-MPC based speed sensorless control of matrix converter fed induction motor drive with zero common mode voltage. IEEE Trans Ind Electron. 2020; 68: 9185-9195.
16. Su J, Gao R, Husain I. Model predictive control based field-weakening strategy for traction EV used induction motor. IEEE Trans Ind Appl. 2018; 54: 2295-2305.
17. Mousavi MS, Davari SA, Nekoukar V, Garcia C, Rodriguez J. A robust torque and flux prediction model by a modified disturbance rejection method for finite set model predictive control of induction motor. IEEE Trans Power Electron. 2021; 36: 9322-9333.
18. Ahmed AA, Koh BK, Lee YI. A comparison of finite control set and continuous control set model predictive control schemes for speed control of induction motors. IEEE Trans Ind Inform. 2018; 14: 1334-1346.
19. Zhang Y, Jin J, Huang L. Model-free predictive current control of PMSM drives based on extended state observer using ultralocal model. IEEE Trans Ind Electron. 2021; 68: 993-1003.
20. Bakeer A, Ismeil MA, Orabi M. A powerful finite control set-model predictive control algorithm for quasi Z-source inverter. IEEE Trans Ind Inform. 2016; 12: 1371-1379.
21. Bakeer A, Ahmed AA. Performance evaluation of PMSM based on model predictive control with field weakening operation and bidirectional quasi Z-source inverter. Proceedings of 2017 Nineteenth International Middle East Power Systems Conference (MEPCON); 2017 December 19-21; Cairo, Egypt. Piscataway, New Jersey, United States: IEEE.
22. Bakeer A, Magdy G, Chub A, Vinnikov D. Predictive control based on ranking multi-objective optimization approaches for a quasi-Z source inverter. CSEE J Power Energy Syst. 2020; 7: 1152-1160.
23. Xu W, Elmorshedy MF, Liu Y, Rodriguez J, Garcia C. Maximum thrust per ampere of linear induction machine based on finite-set model predictive direct thrust control. IEEE Trans Power Electron. 2020; 35: 7366-7378.
24. Elmorshedy MF, Xu W, Liu Y, Dong M. A sensorless finite-set model predictive direct thrust control of a linear induction motor based on MRAS for linear metro. Proceedings of 2019 IEEE

International Electric Machines & Drives Conference (IEMDC); 2019 May 12-15; San Diego, CA, USA. Piscataway, New Jersey, United States: IEEE.
25. Elmorshedy MF, Xu W, Ali MM, Liu Y, Allam SM. High performance speed sensorless finite-set predictive thrust control of a linear induction motor based on MRAS and fuzzy logic controller. Proceedings of 2020 IEEE 9th International Power Electronics and Motion Control Conference (IPEMC2020-ECCE Asia); 2020 November 29-December 02; Nanjing, China. Piscataway, New Jersey, United States: IEEE.
26. Hamad SA, Xu W, Diab A, Ali MM, Bukhari SA. Model predictive voltage control for linear induction machine without weighting factor. Proceedings of 2021 13th International Symposium on Linear Drives for Industry Applications (LDIA); 2021 July 01-03; Wuhan, China. Piscataway, New Jersey, United States: IEEE.
27. Elmorshedy MF, Almakhles DJ, El-Sousy FF. Modified primary flux linkage for enhancing the linear induction motor performance based on sliding mode control and model predictive flux control. IEEE Access. 2023; 11: 26184-26198.
28. Elmorshedy MF, Xu W, Liu Y, Allam SM, Dong M. Speed control of linear induction motor based on finite-set model predictive direct flux control. Proceedings of 2019 IEEE International Symposium on Predictive Control of Electrical Drives and Power Electronics (PRECEDE); 2019 May 31-June 02; Quanzhou, China. Piscataway, New Jersey, United States: IEEE.
29. Elmorshedy MF, Xu W, Ali MM, Bukhari SA. Speed regulation of linear induction motor with finite state predictive thrust control based on sliding mode controller. Proceedings of 2021 13th International Symposium on Linear Drives for Industry Applications (LDIA); 2021 July 01-03; Wuhan, China. Piscataway, New Jersey, United States: IEEE.
30. Elmorshedy MF, Almakhles D, Xu W, Ali JM, Islam MR. Finite state model predictive thrust control based on reduced number of predicted voltage vectors for linear induction motor. Proceedings of 2022 IEEE Global Conference on Computing, Power and Communication Technologies (GlobConPT); 2022 September 23-25; New Delhi, India. Piscataway, New Jersey, United States: IEEE.
31. Duncan J. Linear induction motor-equivalent-circuit model. IEE Proc B. 1983; 130: 51-57.
32. Bakeer A, Alhasheem M. Finite control set-model predictive control synthesized with SVPWM for quasi Z-source inverter. Proceedings of 2021 IEEE 22nd Workshop on Control and Modelling of Power Electronics (COMPEL); 2021 November 02-05; Cartagena, Colombia. Piscataway, New Jersey, United States: IEEE.
33. Bakeer A, Alhasheem M, Peyghami S. Efficient fixed-switching modulated finite control set-model predictive control based on artificial neural networks. Appl Sci. 2022; 12: 3134.
34. Bakeer A, Alhasheem M, Chub A. Improved cost function definition for fixed switching frequency FCS-MPC with SVPWM. Proceedings of 2021 22nd International Middle East Power Systems Conference (MEPCON); 2021 December 14-16; Assiut, Egypt. Piscataway, New Jersey, United States: IEEE.